

Critical dynamics of the simple-cubic Heisenberg antiferromagnet RbMnF_3 : Extrapolation to $q=0$

Shan-Ho Tsai^{a,b} and D. P. Landau^a

^a Center for Simulational Physics, University of Georgia, Athens, GA 30602

^b Enterprise Information Technology Services, University of Georgia, Athens, GA 30602

(Dated: November 7, 2018)

Monte Carlo and spin dynamics simulations have been used to study the dynamic critical behavior of RbMnF_3 , treated as a classical Heisenberg antiferromagnet on a simple cubic lattice. In an attempt to understand the difference in the value of the dynamic critical exponent z between experiment and theory, we have used larger lattice sizes than in our previous simulations to better probe the asymptotic critical region in momentum. We estimate $z = 1.49 \pm 0.03$, in good agreement with the renormalization-group theory and dynamic scaling predictions. In addition, the central peak in the dynamic structure factor at T_c , seen in experiments and previous simulations, but absent in the renormalization-group and mode-coupling theories, is shown to be solely in the longitudinal component.

I. INTRODUCTION

The dynamic critical behavior of RbMnF_3 , a close realization of the isotropic, simple cubic Heisenberg antiferromagnet, has been the subject of several experimental (see Coldea et al¹ and references therein), and theoretical studies^{2,3,4,5,6}. The real time dynamics of this system is governed by coupled equations of motion for the magnetic ions. In the classification of Hohenberg and Halperin⁵, the critical dynamics of this system pertains to class G, for which the order parameter (the staggered magnetization) is not conserved.

Dynamic critical behavior can be characterized by a dynamic critical exponent z , and for RbMnF_3 the most precise experimental estimate¹ is $z = 1.43 \pm 0.04$. This estimate is slightly below the predicted value^{3,4,5,6} of $z = 1.5$ for an isotropic three-dimensional Heisenberg antiferromagnet. Our previous estimate using spin-dynamics simulation⁷ (obtained before we knew the latest experimental result¹) was $z = 1.43 \pm 0.03$ in good agreement with the experimental value. The slight disagreement between theory and both the experiment and the simulation was perplexing, but one possible explanation was that neither of these latter studies probed the asymptotic critical region sufficiently far. To check this, neutron scattering experiments would have to be performed with smaller momentum transfer q , a task that can be quite challenging. We can also resort to spin dynamics simulations of the model on larger lattice sizes which allow access to smaller q values.

Spin dynamics simulations⁸ have proven to be an effective tool to study dynamic behavior of magnetic systems. Direct and quantitative comparisons of magnetic excitation dispersion curves and dynamic structure factor line shapes from experiment¹ and spin dynamics simulations have shown good agreement, with no adjustable parameters^{7,9}. At the critical temperature T_c , both experiment and simulation find that the average dynamic structure factor $S(\mathbf{q}, \omega)$, for momentum \mathbf{q} and frequency ω , has a spin-wave peak and an additional central

peak not predicted by either the renormalization-group theory³ or mode-coupling theory⁴. In a polarized neutron scattering experiment¹⁰ below T_c , the quasi-elastic peak has been shown to be longitudinal in character. It is thus interesting to investigate whether the central peak at T_c originates in the longitudinal, in the transverse or in both components with respect to the staggered magnetization. Another motivation for separating the longitudinal and transverse components of the dynamic structure factor is to test the theoretical prediction² that below T_c the longitudinal momentum-dependent susceptibility behaves as $\chi^L(q) \sim 1/q$, whereas the q -dependence of the transverse component is $\chi^T(q) \sim 1/q^2$. Although experimental measurements¹ are consistent with $\chi^L(q) \sim 1/q$, the lack of reliable small wave vector measurements hindered a conclusive experimental test of this predicted divergence. The experimental value for the transverse component is $\chi^T(q) \sim 1/q^{1.91 \pm 0.05}$.

In this paper we use spin dynamics simulations to study the dynamic critical behavior of the isotropic Heisenberg antiferromagnet on the simple cubic lattice, using larger lattices than in our previous simulations, as motivated above. We investigate the longitudinal and transverse components of the dynamic structure factor, and compare the q -dependence of the susceptibility with the predicted forms both at and below T_c . For brevity, we do not present our methodology in great detail here; it has been described in earlier work^{7,8}.

II. MODEL AND METHODS

We consider three-dimensional classical spins $\mathbf{S}_\mathbf{r}$ of unit length, defined on the sites \mathbf{r} of $L \times L \times L$ simple cubic lattices. The interaction is described by a model Hamiltonian written as

$$\mathcal{H} = J \sum_{\langle \mathbf{r}\mathbf{r}' \rangle} \mathbf{S}_\mathbf{r} \cdot \mathbf{S}_{\mathbf{r}'}, \quad (1)$$

where the summation is over pairs of nearest-neighbor spins, and $J > 0$ is an antiferromagnetic exchange

coupling. An earlier high-resolution Monte Carlo simulation¹¹ determined $T_c = 1.442929(77)J$, so any uncertainty in the location of the critical temperature of this model is negligible.

The dynamics of the spins is governed by coupled equations of motion⁸ and the dynamic structure factor $S^k(\mathbf{q}, \omega)$ is given by the Fourier transform of the space- and time-displaced correlation functions $C^k(\mathbf{r} - \mathbf{r}', t) = \langle S_{\mathbf{r}}^k(t) S_{\mathbf{r}'}^k(0) \rangle - \langle S_{\mathbf{r}}^k(t) \rangle \langle S_{\mathbf{r}'}^k(0) \rangle$, where k represents the spin components. The coupled equations of motion were integrated using an algorithm¹² based on 4th-order Suzuki-Trotter decompositions of exponential operators, with a time step dt . The integrations were performed up to time t_{max} , starting from equilibrium configurations at temperature T generated with a hybrid Monte Carlo method⁷. The correlations $C^k(\mathbf{r} - \mathbf{r}', t)$ were computed for time displacements ranging from 0 to t_{cutoff} and the canonical ensemble was established by averaging results from N different initial equilibrium configurations. We used periodic boundary conditions in space and thus we could only access a set of discrete values of momentum transfer given by $q = 2\pi n_q/L$, where $n_q = 1, 2, \dots, L/2$. Because of computer memory limitations we restricted our data to $\mathbf{q} = (q, 0, 0)$, $(q, q, 0)$, and (q, q, q) , which correspond to the [100], [110], and [111] directions, respectively.

In an attempt to probe the true asymptotic critical region in momentum and thus provide a more accurate estimate of the dynamic critical exponent, we extended our Monte Carlo¹³ and spin-dynamics simulations^{7,8} to systems as large as $L = 72$ at T_c . For $L = 72$, each equilibrium configuration was generated with 2500 hybrid Monte Carlo steps, each of which consists of two Metropolis sweeps through the lattice and eight overrelaxation steps. We used $dt = 0.2/J$, $t_{max} = 1080/J$, $t_{cutoff} = 1000/J$, and $N = 1000$. We have also improved the statistics of our previous simulations for $L = 48$ and 60 by increasing the number of initial configurations to $N = 1000$. With $L = 72$, the smallest wave vector that we can access is $q = 2\pi/72 = 2\pi(0.0139)$, whereas, in our units, the smallest q value probed by experiment¹ was $q = 2\pi(0.02)$.

The dynamic critical exponent z can be extracted using dynamic finite-size scaling⁸, which yields $\omega \bar{S}^k(\mathbf{q}, \omega) / \bar{\chi}^k(\mathbf{q}) = G(\omega L^z, qL, \delta_\omega L^z)$ and $\bar{\omega}_m^k = L^{-z} \bar{\Omega}^k(qL, \delta_\omega L^z)$, where k represents the polarization, $\bar{S}^k(\mathbf{q}, \omega)$ is the dynamic structure factor convoluted with a Gaussian resolution function with parameter δ_ω , $\bar{\chi}^k(\mathbf{q})$ is the total integrated intensity, and $\bar{\omega}_m^k$ is a characteristic frequency, defined by $\int_{-\bar{\omega}_m^k}^{\bar{\omega}_m^k} \bar{S}^k(\mathbf{q}, \omega) d\omega / 2\pi = \bar{\chi}^k(\mathbf{q}) / 2$. If we set $\delta_\omega = 0$ the exponent z can be obtained from the slope of a graph of $\ln(\bar{\omega}_m^k)$ vs $\ln(L)$, at fixed qL . To test the robustness of the estimate, we have also used $\delta_\omega = 0.005(72/L)^z$, and determined z iteratively^{7,8}. As in our previous work^{7,9}, the dynamic critical exponent is estimated using the average dynamic structure factor.

After understanding the difference in the dynamic critical exponent between experiment and theory, we can ex-

amine other unresolved issues, such as the nature of the central peak at T_c observed in experiments, but absent in theoretical studies. To this end, we analyzed longitudinal and transverse motions of the spins with respect to the staggered magnetization. The dynamics of the isotropic Heisenberg model, given by the coupled equations of motion, conserves both the total energy and the uniform magnetization, which is the order parameter for the Heisenberg ferromagnet. However, for the antiferromagnet the order parameter (staggered magnetization) is not a constant of the motion; therefore, separating components of the spin parallel (longitudinal component) and perpendicular (transverse component) to the order parameter is challenging. Our approach to determine the individual components of the spin motion, and thus of $S(\mathbf{q}, \omega)$, was to rotate the frame of reference to align the z -axis parallel to the staggered magnetization before starting the time integrations, to make the z -axis coincide with the longitudinal direction. As we integrated the equations of motion, the direction of the staggered magnetization changed slightly because it is not a conserved quantity. Therefore, after each integration step we re-rotated the frame of reference to re-align the z -axis with the staggered magnetization, thereby restoring the z -axis as the longitudinal direction. In this part of our simulations we used $L = 24$ with $t_{max} = 480/J$, $t_{cutoff} = 400/J$, $dt = 0.2/J$, and $N = 12,000$, in addition to $L = 36, 48$, and 60 , with $t_{max} = 880/J$, $t_{cutoff} = 800/J$, $dt = 0.2/J$, and $N = 11,000, 7,000$, and $3,000$, respectively. We denote the longitudinal and transverse components of $S(\mathbf{q}, \omega)$ as $S^L(\mathbf{q}, \omega)$ and $S^T(\mathbf{q}, \omega)$, respectively.

We have also investigated $\chi^L(q)$ and $\chi^T(q)$, the integrated intensities of $S^L(\mathbf{q}, \omega)$ and $S^T(\mathbf{q}, \omega)$, respectively. When the decay of the dynamic structure factor is slow, as is the case of $S^T(\mathbf{q}, \omega)$ at T_c , computing the integrated intensity is complicated by the fact that at high frequencies $[\pi/(2dt) \lesssim \omega \lesssim \pi/dt]$ the approximation of the integral Fourier transform as a discrete sum is highly dependent on the summation method (e.g. direct sum, trapezoidal rule, Simpson's rule, etc.). In terms of cpu time usage, it is more efficient to integrate the equations of motion with the largest time step dt that still yields a stable method and accurate time evolutions; however, the maximum accessible frequency is inversely proportional to dt . Simulations for $L = 24$ at T_c using a smaller time step ($dt = 0.1/J$) showed that both the Simpson's rule and the trapezoidal rule produce consistent results for $S^L(\mathbf{q}, \omega)$ and $S^T(\mathbf{q}, \omega)$ up to $\omega \approx 15J$. A direct comparison between the dynamic structure factor obtained with $dt = 0.1/J$ and that obtained with the Simpson's rule and the trapezoidal rule using $dt = 0.2/J$ up to $\omega \approx 15J$ shows that the trapezoidal rule gives a better approximation for $S^L(\mathbf{q}, \omega)$ and $S^T(\mathbf{q}, \omega)$ at high frequencies. Estimates of $\chi^L(q)$ and $\chi^T(q)$ are not significantly dependent on the methods used to integrate $S^L(\mathbf{q}, \omega)$ and $S^T(\mathbf{q}, \omega)$, respectively, and we use Simpson's rule for these integrations.

Our approach to determine $\chi^T(q)$ at T_c was to compute $S^T(\mathbf{q}, \omega)$ with the trapezoidal rule and then to integrate it from $\omega = 0$ to $8J$. Although the intensity of $S^T(\mathbf{q}, \omega)$ has not decayed to zero at $\omega = 8J$, it is a small fraction of the intensity of the spin-wave peak. Data for $\omega = 4J$ to $8J$ were fitted with an exponential function, which was then used in the integration to $\omega = \infty$. (An exponential function was chosen for this fitting because it is the simplest one that yielded a good fitting in the range of frequency used.) To estimate the longitudinal component $\chi^L(q)$ at T_c we simply used the trapezoidal rule to determine $S^L(\mathbf{q}, \omega)$ and then integrated it from $\omega = 0$ to $\omega = 10J$, without further high-frequency corrections, because $S^L(\mathbf{q}, \omega)$ decays quickly in frequency.

The behavior of $\chi^T(q)$ and $\chi^L(q)$ below T_c is studied with spin dynamics simulations at $T = 0.5T_c$ using $dt = 0.2/J$ and $L = 24$ and 36 , with $N = 1000$ for each lattice size. At this temperature both $S^L(\mathbf{q}, \omega)$ and $S^T(\mathbf{q}, \omega)$ decay quickly, hence these line shapes were obtained with the trapezoidal rule and they were then integrated from $\omega = 0$ to $\omega = 10J$.

For comparison, we have also computed the longitudinal and transverse components of $S(\mathbf{q}, \omega)$ with respect to the residual uniform magnetization. In this case, the rotation of the frame of reference to align one axis parallel to the uniform magnetization was only required once, before starting the time integrations, because the uniform magnetization vector is conserved.

III. RESULTS

Our results for the average dynamic structure factor $S(\mathbf{q}, \omega)$ show a spin wave and a central peak for $T \leq T_c$. The spin wave dispersion curve for $L = 72$, $T = T_c$ and \mathbf{q} vectors in the $[100]$ direction, shown in Fig.1, was obtained by fitting $S(\mathbf{q}, \omega)$ with Lorentzian spin-wave creation and annihilation peaks centered at $\omega = \pm\omega_s$, and a Lorentzian peak at $\omega = 0$. We have obtained reasonable fittings for q values corresponding to $n_q = 1$ to 7 ; for larger n_q , the spin-wave line shapes were not Lorentzian and the positions of the spin-wave peaks ω_s were read off directly without any fitting. We remind the reader that the first Brillouin zone edge in the $[100]$ direction occurs at $n_q = L/2$. An estimate of the dynamic critical exponent z is obtained by fitting the dispersion curve with a function⁵ $\omega_s = Dn_q^z$. Since the asymptotic critical region corresponds to small values of q , we have used $n_q = 1$ to 9 in the fitting (dashed line in Fig.1), and obtained $z = 1.35 \pm 0.05$. If $n_q = 1$ is excluded due to its large finite-size effect⁷, the fitting yields $z = 1.45 \pm 0.07$ (solid line in Fig.1).

A better approach to determine z is to use the dynamic finite-size scaling theory outlined above. Using this method, we obtained z for different values of n_q , with no resolution function. Such estimates are denoted as z_q and are shown in Fig.2. In our previous work⁷, we estimated z as the average value obtained using $n_q = 1$ and

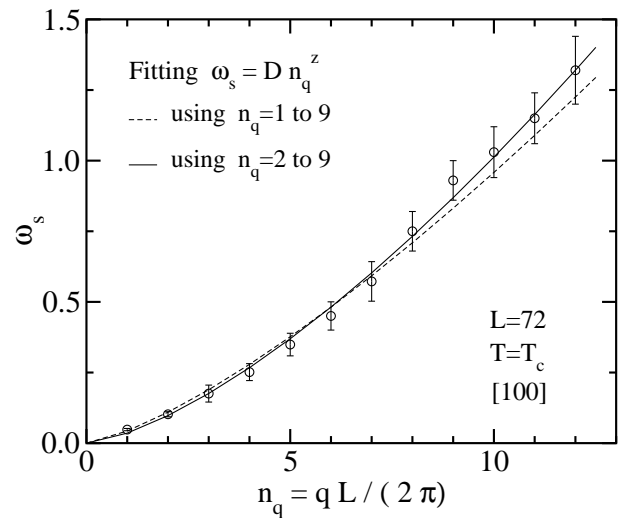


FIG. 1: Spin-wave dispersion curve for the average dynamic structure factor.

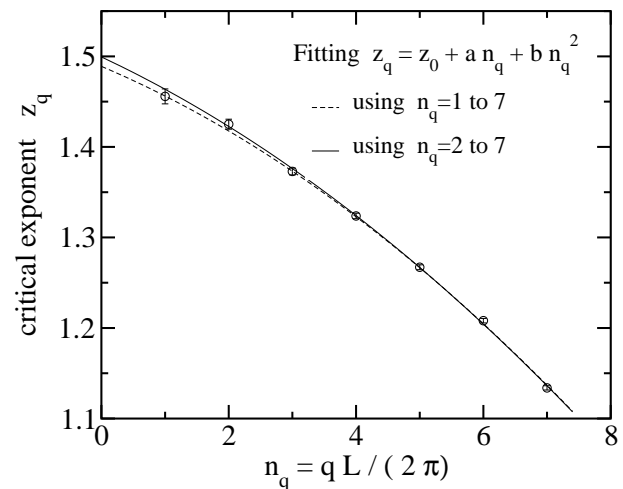


FIG. 2: Estimate of the dynamic critical exponent for different n_q . Analysis done with $L = 30, 36, 48, 60$, and 72 .

$n_q = 2$, with a maximum lattice size of $L = 60$. We now have larger L and better statistics, and hence the present $n_q = 1$ and $n_q = 2$ correspond to q -values that are closer to the asymptotic critical region. Nevertheless, Fig.2 shows that these values of q are not yet in the asymptotic critical region, and a better estimate of z is given by z_0 , obtained by extrapolating z_q to the limit $q \rightarrow 0$. We fitted z_q with the function $z_q = z_0 + an_q + bn_q^2$, where z_0 , a , and b are fitting parameters. Using $n_q = 1, 2, \dots, 7$ in the fitting (dashed line in Fig.2) we find $z_0 = 1.48 \pm 0.02$ and excluding $n_q = 1$, due to its large finite-size dependence, (solid line in Fig.2) we find $z_0 = 1.50 \pm 0.02$. Both estimates agree with the theoretical prediction of $z = 1.5$. Dynamic finite-size scaling theory with a small resolution function was used to determine z_q iteratively. The results thus obtained are within a one- σ error bar of the respective $\delta_\omega = 0$ estimates.

The longitudinal and transverse components of the dynamic structure factor with respect to the staggered magnetization are shown in Figs.3a and 3b, respectively, for $L = 36$, $T = 0.5T_c$ and \mathbf{q} in the [100] direction with $n_q = 3$. While the transverse component has a pro-

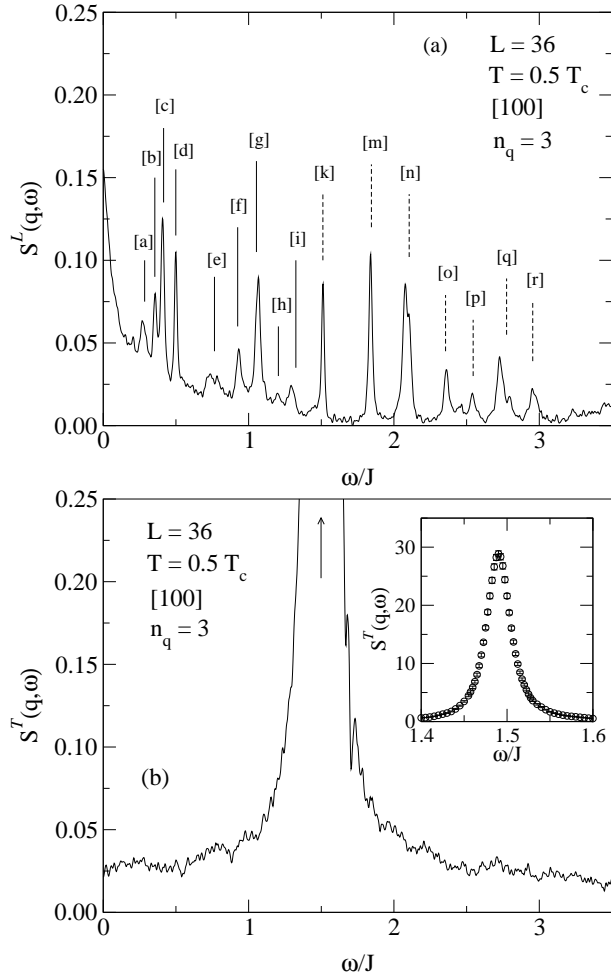


FIG. 3: (a) Longitudinal and (b) transverse components of $S(q, \omega)$, with respect to the staggered magnetization, with $\delta_\omega = 0.005$ at $T = 0.5T_c$. Beside a central peak, the longitudinal component has two-spin-wave subtraction (indicated by solid lines) and addition peaks (dashed lines), corresponding to $18\mathbf{q}_1/\pi$ equal to [a] (2,2,0), [b] (1,1,1), [c] (1,1,0), [d] (1,0,0), [e] (3,2,0), [f] (3,1,1), [g] (3,1,0), [h] (4,1,1), [i] (2,1,1), [k] (1,0,0), [m] (1,1,0), [n] (1,1,1) and (3,1,0), [o] (3,1,1), [p] (2,2,0), [q] (2,1,1) and (3,2,0), [r] (3,2,1) and (4,1,1).

nounced single spin-wave excitation at $\omega/J \approx 1.49$ and intensity ~ 30 , as shown in the inset in Fig.3b, the structures on $S^L(\mathbf{q}, \omega)$ have much smaller amplitudes and comprise a central peak, and a series of two-spin-wave subtraction (a-i) and addition (k-r) peaks. Denoting the momentum and frequency of two single spin waves as (\mathbf{q}_1, ω_1) and (\mathbf{q}_2, ω_2) , the excitations resulting from their addition and subtraction have frequencies $\omega_+ = \omega_1 + \omega_2$ and $\omega_- = |\omega_1 - \omega_2|$, respectively, and momentum $\mathbf{q} = \mathbf{q}_1 + \mathbf{q}_2$. For odd values of n_q there are no

two spin-wave peaks at $\omega = 0$ so the central peak seen in $S^L(\mathbf{q}, \omega)$ is presumably due to spin diffusion.

At T_c , $S^L(\mathbf{q}, \omega)$ (see Fig.4a) seems to be predominantly diffusive with a central peak that is much more intense than the spin-wave peak in $S^T(\mathbf{q}, \omega)$ (Fig.4b). These data provide clear evidence that the central peak in the average $S(\mathbf{q}, \omega)$ at T_c , seen in experiment and previous simulations, but not present in renormalization-group and mode-coupling theories, appears only in the longitudinal component. Two spin-wave excitations at T_c cannot be resolved.

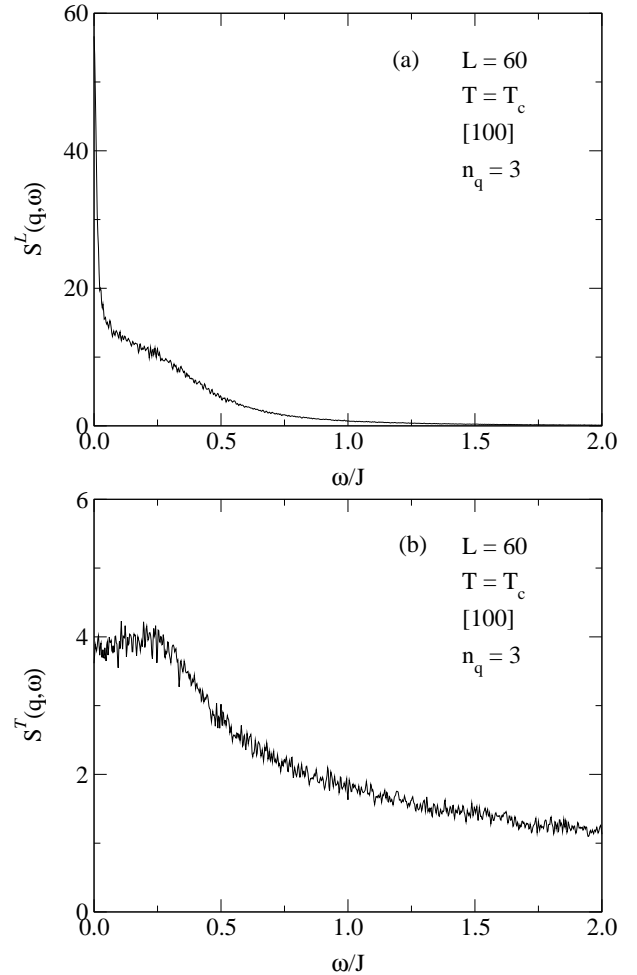


FIG. 4: (a) Longitudinal and (b) transverse components of $S(q, \omega)$, with respect to the staggered magnetization at T_c .

Figure 5 shows log-log plots of $\chi^L(q)$ and $\chi^T(q)$, the integrated intensities of $S^L(q, \omega)$ and $S^T(q, \omega)$, respectively, as a function of momentum in the [100] direction. The momentum dependence of the integrated intensity has the form q^{-x} . At $T = 0.5T_c$ (Fig.5a), a linear fitting in the log-log plane of $\chi^L(q)$ and $\chi^T(q)$ versus n_q for $L = 36$ using $n_q = 1$ to 6 gives $\chi^L \sim 1/q^{0.80 \pm 0.16}$ and $\chi^T \sim 1/q^{1.94 \pm 0.06}$, whereas if the $n_q = 1$ point is dropped the linear fitting yields (solid lines) $\chi^L \sim 1/q^{0.88 \pm 0.35}$ and $\chi^T \sim 1/q^{1.92 \pm 0.10}$. These results are in agreement with both renormalization-group theory prediction² and

experimental results¹. We have also tried to fit $\chi^L(q)$ with the Ornstein-Zernike mean-field formula¹⁴ $\chi^L(q) = \chi^L(0) \kappa^2 / (q^2 + \kappa^2)$, using $\chi^L(0)$ and κ as fitting parameters; however, this expression did not yield a good fitting. At T_c (Fig.5b), our data for $L = 60$ indicate that

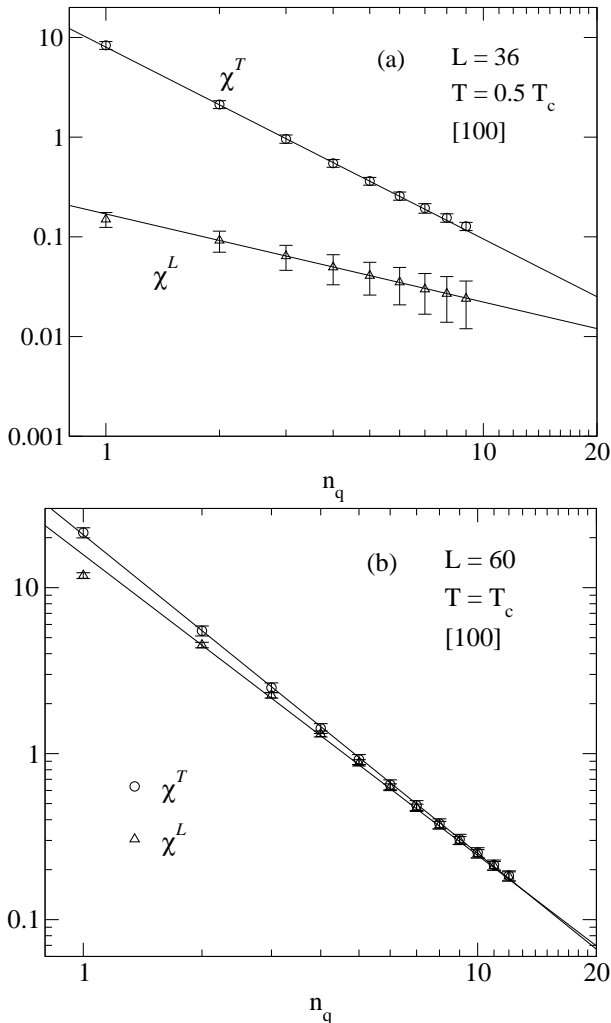


FIG. 5: Log-log plot of the longitudinal (Δ) and transverse (\circ) integrated intensity as a function of n_q , at (a) $T = 0.5T_c$ and (b) $T = T_c$. The solid lines are linear fittings using $n_q = 2$ to $n_q = 6$ for (a), and to $n_q = 10$ for (b).

$\chi^L \sim 1/q^{1.81 \pm 0.03}$ and $\chi^T \sim 1/q^{1.92 \pm 0.04}$, where $n_q = 2$ to 10 have been used in the fitting. Finite-size effects on the low- q divergence exponents of χ^L and χ^T at T_c are shown in Fig.6. A linear fitting of these exponents as a function of $1/L$ yields $\chi^L \sim 1/q^{1.88 \pm 0.05}$ and $\chi^T \sim 1/q^{1.95 \pm 0.07}$ for the thermodynamic limit where $L = \infty$. The dynamic scaling prediction for the static susceptibility at T_c is^{6,15} $\chi = 1/q^{2-\eta}$, where for the purpose of this comparison we can use¹⁶ $\eta \approx 0.04 \pm 0.01$. We see that while χ^T is consistent with the dynamic scaling prediction, our large error bars do not exclude the mean-field behavior of $\chi \sim 1/q^2$. Our estimate for the divergence of χ^L at small q is slightly less rapid than predicted, but still consistent

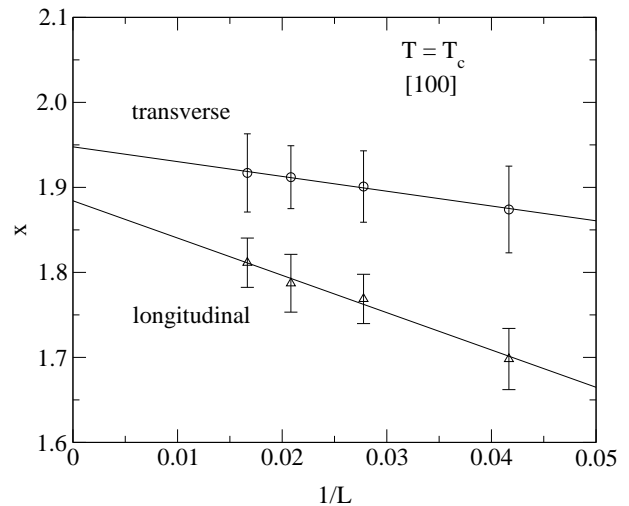


FIG. 6: Low- q divergence exponents of χ^L (Δ) and χ^T (\circ) at T_c , as a function of the inverse lattice linear size. The solid lines are linear fittings using data for $L = 24, 36, 48, 60$.

with it within a two- σ error bar.

Figure 7 shows a log-log plot of the longitudinal and transverse components of the characteristic frequency as a function of L , for $n_q = 2$ and $\delta_\omega = 0$ at T_c . These components are denoted as ω_m^L and ω_m^T , respectively, and according to dynamic finite-size scaling we have $\omega_m^L = L^{-z^L} \Omega^L(qL)$ and $\omega_m^T = L^{-z^T} \Omega^T(qL)$. For $n_q = 2$ (see Fig.7) we obtain $z^L = 1.48 \pm 0.14$ and $z^T = -0.03 \pm 0.25$, where data for $L = 36, 48$, and 60 have been included in the analysis. Our data show that the dynamic critical exponent for the transverse component is consistent with $z = 0$, indicating that this component is not critical. In contrast, the longitudinal component is critical, with $z \approx 1.5$.

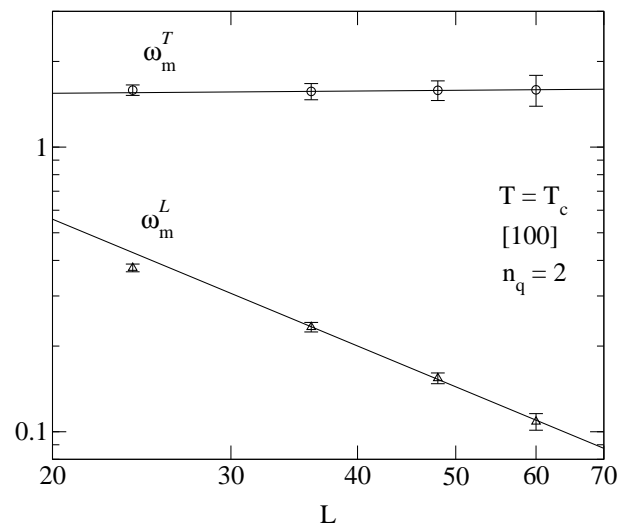


FIG. 7: Log-log plot of the longitudinal (Δ) and transverse (\circ) components of the characteristic frequency as a function of L with $\delta_\omega = 0$.

Separating $S(\mathbf{q}, \omega)$ into longitudinal and transverse components with respect to the uniform magnetization we see that the longitudinal component has a central peak, a pronounced spin-wave peak and less intense two-spin-wave peaks. In contrast, each such peak in the transverse component is split into two peaks, with frequencies $\omega^L \pm \Delta\omega$, where ω^L is the frequency of the corresponding peak in the longitudinal component of $S(\mathbf{q}, \omega)$. The shift $\Delta\omega$ in the peak frequencies corresponds to the frequency of oscillation of the staggered magnetization.

IV. CONCLUSIONS

We have used Monte Carlo and spin dynamics simulations to study the dynamic behavior of the isotropic Heisenberg antiferromagnet on the simple cubic lattice. When we use the same range of momentum q as probed by experiment¹, the dynamic critical exponent obtained⁷ is in good agreement with its experimental value, which is slightly lower than theoretical predictions. In our present work we have used a larger lattice size, and thus smaller values of q , in addition to obtaining better statistics and extrapolating finite q results to the limit $q = 0$. This allowed us to study systematic changes as we approach the asymptotic critical region and our improved estimate (*i.e.* with systematic errors largely eliminated) is $z = 1.49 \pm 0.03$, in good agreement with the renormalization group theory and dynamic scaling predictions. Presumably the values of q used in the experiment¹ and in our previous simulations were not in the true asymptotic critical region, resulting in a slightly lower estimate of z . This should serve as a warning for future simulational and experimental probes of dynamic critical behavior.

Longitudinal and transverse components of $S(\mathbf{q}, \omega)$ with respect to the staggered magnetization are investigated separately. This required rotation of the frame of reference after each integration step because the stag-

gered magnetization is not a conserved quantity. Below T_c , the transverse component $S^T(\mathbf{q}, \omega)$ has a pronounced spin-wave peak, whereas the longitudinal component $S^L(\mathbf{q}, \omega)$ is dominated by two-spin-wave addition and subtraction peaks, and a central peak presumably due to spin diffusion. These results are consistent with theory² and experiment¹⁰, both of which have shown that the transverse spin fluctuations are propagating, dominated by spin-waves, whereas the quasielastic peak is due to longitudinal fluctuations. At T_c , $S^L(\mathbf{q}, \omega)$ has a central peak that is much more intense than the spin-wave peak in $S^T(\mathbf{q}, \omega)$ and no central peak was seen in $S^T(\mathbf{q}, \omega)$. Explaining the appearance of a central peak in $S^L(\mathbf{q}, \omega)$ at T_c remains a challenge for theory. We have also seen that while $S^T(\mathbf{q}, \omega)$ is not critical, $S^L(\mathbf{q}, \omega)$ is critical and it has a dynamic critical exponent $z \approx 1.5$.

These findings further support our earlier conclusion that a simple, nearest-neighbor, isotropic Heisenberg model describes the behavior of RbMnF₃ quite well. The only limitations in the agreement appear to be at T_c , and even there all qualitative features and dynamic exponent are faithfully reproduced.

Below T_c our results for the longitudinal and transverse components of the integrated intensities of $S(\mathbf{q}, \omega)$ are consistent with renormalization-group theory predictions, and not with the mean-field one. In contrast, at T_c , while the integrated intensities are consistent with the renormalization-group theory prediction, the large error bars do not allow us to exclude the mean-field behavior.

V. ACKNOWLEDGMENTS

Fruitful discussions with A. Cuccoli are gratefully acknowledged. This research was partially supported by NSF grant DMR-0094422. Simulations were performed on the Cray T90 at SDSC and on the IBM SP at the U. of Michigan.

¹ R. Coldea, R.A. Cowley, T.G. Perring, D.F. McMorrow, and B. Roessli, Phys. Rev. B **57**, 5281 (1998).

² G.F. Mazenko, M.J. Nolan, and R. Freedman, Phys. Rev. B **18**, 2281 (1978).

³ R. Freedman and G.F. Mazenko, Phys. Rev. Lett. **34**, 1575 (1975); Phys. Rev. B **13**, 4967 (1976).

⁴ A. Cuccoli, S.W. Lovesey, and V. Tognetti, J. Phys.: Condens. Matter **6**, 7553 (1994).

⁵ P.C. Hohenberg and B.I. Halperin, Rev. Mod. Phys. **49**, 435 (1977).

⁶ B.I. Halperin and P.C. Hohenberg, Phys. Rev. **177**, 952 (1969).

⁷ S.-H. Tsai, A. Bunker, and D.P. Landau, Phys. Rev. B **61**, 333 (2000).

⁸ D.P. Landau and M. Krech, J. Phys.: Condens. Matter **11**, R179 (1999).

⁹ D.P. Landau, S.-H. Tsai, and A. Bunker, J. Magn. Magn. Mat. **226-230**, 550 (2001); J. Phys. Soc. Jpn. **69** Suppl.

A, 407 (2000); D.P. Landau, A. Bunker, H.G. Evertz, M. Krech, and S.-H. Tsai, Prog. Theor. Phys. Suppl. **138**, 423 (2000).

¹⁰ U.J. Cox, R.A. Cowley, S. Bates, and L.D. Cussen, J. Phys.: Condens. Matter **1**, 3031 (1989).

¹¹ K. Chen, A.M. Ferrenberg, and D.P. Landau, Phys. Rev. B **48**, 3249 (1993).

¹² M. Krech, A. Bunker and D.P. Landau, Comput. Phys. Commun. **111**, 1 (1998).

¹³ See e.g., D.P. Landau and K. Binder, *A Guide to Monte Carlo Simulations in Statistical Physics* (Cambridge University Press, 2000).

¹⁴ See e.g., M.F. Collins, *Magnetic Critical Scattering* (Oxford University Press, 1989).

¹⁵ D.S. Ritchie and M.E. Fisher, Phys. Rev. B **5**, 2668 (1972).

¹⁶ M. Campostrini, M. Hasenbusch, A. Pelissetto, P. Rossi, and E. Vicari, Phys. Rev. B **65**, 144520 (2002).